CANCER IMMUNOLOGY

The immune system profoundly restricts intratumor genetic heterogeneity

Idan Milo[1,2], Marie Bedora-Faure[3], Zacarias Garcia[1,2], Ronan Thibaut[1,2,4], Leïla Périé[5,6], Guy Shakhar[7], Ludovic Deriano[3], Philippe Bousso[1,2]*

Tumors develop under the selective pressure of the immune system. However, it remains critical to establish how the immune system affects the clonal heterogeneity of tumors that often display cell-to-cell variation in genetic alterations and antigenic expression. To address these questions, we introduced a multicolor barcoding strategy to study the growth of a MYC-driven B cell lymphoma harboring a large degree of intratumor genetic diversity. Using intravital imaging, we visualized that lymphoma subclones grow as patches of sessile cells in the bone marrow, creating a spatially compartmentalized architecture for tumor diversity. Using multicolor barcoding and whole-exome sequencing, we demonstrated that immune responses strongly restrict intratumor genomic diversity and favor clonal dominance, a process mediated by the selective elimination of more immunogenic cells and amplified by epitope spreading. Anti–PD-1 treatment also narrowed intratumor diversity. Our results provide direct evidence that immune pressure shapes the level of intratumor genetic heterogeneity and have important implications for the design of therapeutic strategies.

INTRODUCTION

Cancer development results from a complex evolutionary process fueled, in large part, by stochastic genomic alterations and outgrowth of subclones endowed with selective survival and proliferative advantages in the tumor microenvironment (*1*, *2*). These processes often proceed in a branched manner (*3*), with distinct subclones developing in parallel, generating considerable genetic and functional diversity within the tumor of a given patient (*4*–*6*). How this diversity is structured at the anatomical and microanatomical level has yet to be fully understood for each cancer. Understanding the shaping of intratumor heterogeneity is essential not only because it encompasses fundamental mechanisms of tumor evolution but also because it may have profound consequences on therapeutic response (*5*). Genomic instability, cell autonomous fitness, and microenvironmental constraints are well-characterized factors that influence the level of tumor heterogeneity (*4*, *6*). The immune system can also impose pressure on tumor cells (*7*). In this model, referred to as tumor editing, tumor cells are initially eliminated by the immune response as part of a process that will favor the emergence of cells invisible to the immune system. Evidence for immune-edited tumors has been provided by several groups (*8*). However, the overall impact of immune surveillance on intratumor heterogeneity is not known. It is, for example, unclear whether each subclone is subjected to immunoediting, a process that should maintain overall diversity. Alternatively, immune responses may promote genomic instability in tumor cells, favoring the emergence of new subclones and thus the possibility of increasing tumor heterogeneity (*9*). Last, immune responses could act primarily by eliminating the progeny of most subclones and selecting the residual subclones, thus diminishing intratumor diversity.

In addition, the contribution of various immune mechanisms involved in shaping tumor diversity remains to be established. A potentially critical consequence of intratumor diversity on immune responses lies in the mosaic expression of tumor antigen. Tumor antigens are often detected in only a fraction of tumor cells, a phenomenon that potentially constitutes a strong limitation for successful establishment of antitumor immunity (*10*–*12*). Addressing these important questions experimentally is somewhat complicated by the paucity of methods to dynamically track intratumor diversity. Here, we develop a multicolor labeling strategy to visualize and analyze the diversity within a MYC-driven B cell lymphoma in the bone marrow. Using this approach, we examined how tumor heterogeneity is regulated in time and space and established mechanisms by which the immune response can profoundly restrict intratumor diversity.

RESULTS

A mouse model of spontaneous B cell lymphoma exhibits extensive intratumor genetic diversity

To evaluate the extent of genetic heterogeneity in a developing tumor, we relied on the Eμ-myc transgenic mouse model (*13*). These animals express the *c-myc* oncogene under the control of the immunoglobulin heavy chain enhancer and spontaneously develop B cell lymphoma after a few months of age. Tumors isolated from five individual mice were subjected to chromosomal analysis using spectral karyotyping (SKY). As shown in Fig. 1 and fig. S1, we observed large diversity in the genetic alterations of each tumor including chromosome gains/losses and translocations. Within a given mouse, virtually all tumor cells shared specific chromosomal alterations. These shared alterations were unique to each mouse analyzed, strongly suggestive of a common ancestor and most probably reflecting stochastic events in the transformation process and tumor evolution. Within a given mouse, individual tumor cells also displayed distinct genetic modifications indicative of further diversification. For example, within tumor cells isolated from a male Eμ-myc transgenic mouse (Fig. 1C, lymphoma #1), virtually all cells displayed three copies of chromosomes 3 and 5, whereas around 28, 5, and 5% of the cells had lost the Y chromosome, one copy of chromosome 8, and one copy of chromosome 19, respectively. Similar features were observed in the other tumors analyzed (Fig. 1C and fig. S1). Chromosome loss events were documented in a large fraction (42 to 100%) of the various chromosomes (fig. S2). Overall, these results establish the extensive

[1]Dynamics of Immune Responses Unit, Equipe Labellisée Ligue Contre le Cancer, Institut Pasteur, 75015 Paris, France. [2]INSERM U1223, 75015 Paris, France. [3]Genome Integrity, Immunity and Cancer Unit, Department of Immunology, Department of Genomes and Genetics, Institut Pasteur, 75015 Paris, France. [4]University Paris Diderot, Sorbonne Paris Cité, Cellule Pasteur, rue du Dr Roux, 75015 Paris, France. [5]Institut Curie, PSL Research University, CNRS UMR168, 11 rue Pierre et Marie Curie, 75005 Paris, France. [6]Sorbonne Universités, UPMC University Paris 06, 4 place Jussieu, 75005 Paris, France. [7]Department of Immunology, Weizmann Institute of Science, Rehovot 76100, Israel. *Corresponding author. Email: philippe.bousso@pasteur.fr

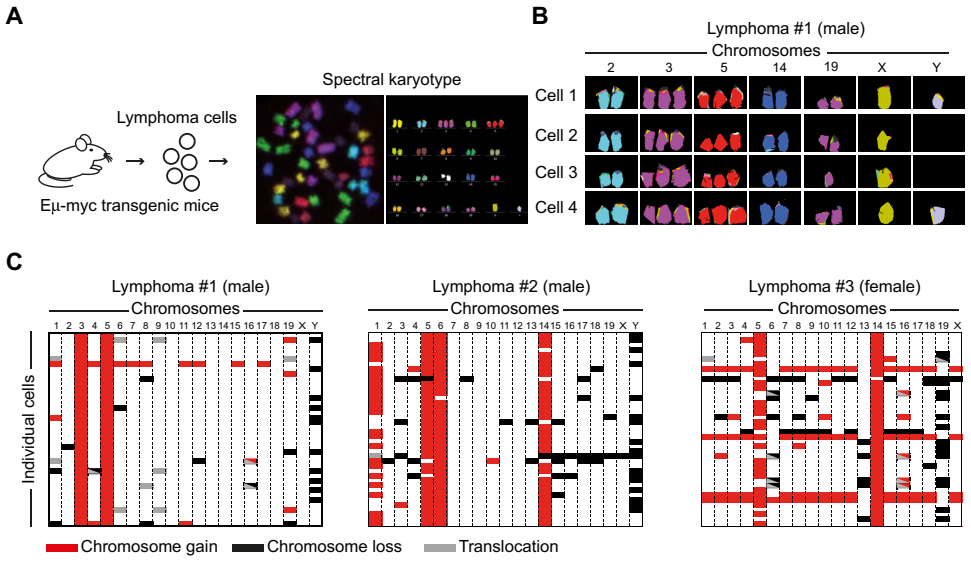

Fig. 1. Lymphoma B cells developing in Eμ-myc transgenic mice display extensive intratumor genetic diversity. (**A**) Experimental setup. Lymphoma cells were isolated from the lymphoid organs of Eμ-myc transgenic mice. Metaphases were prepared, and 20 to 50 cells from each individual tumor were subjected to SKY. (**B** and **C**) Genetic heterogeneity in different cells isolated from the same tumor. (B) Representative images of various chromosomes obtained from four individual cells from one tumor. (C) Tables recapitulating the karyotypes of 40 cells analyzed from each individual tumor. Each table corresponds to the tumor cells isolated from one mouse. Red represents gain of chromosomes, black represents loss of chromosomes, and gray shows translocations. Data are representative of a total of five tumors isolated from male or female tumor-bearing Eμ-myc mice.

genetic intratumor heterogeneity in MYC-driven B cell lymphomas and illustrate the frequent loss of chromosomes, a process that could potentially translate into mosaic expression of tumor antigens.

A multicolor barcoding strategy allows the analysis and visualization of tumor clonal diversity

The intratumor heterogeneity observed in this B cell lymphoma raises fundamental questions of how this diversity is established and further evolves in situ. To address these questions, we developed a multicolor barcoding strategy, adapted from the previously described fluorescent marking method (*14*, *15*), with the aim to visualize and measure clonal heterogeneity. In brief, lymphoma cells isolated from an individual Eμ-myc transgenic mouse were retrovirally transduced to express distinct fluorescent proteins or a combination of two proteins (Fig. 2A). Cells with different color combinations were sorted and mixed. Five clearly distinguishable equally distributed populations were reproducibly generated in the initial mix (fig. S3A). Each colored population exhibited the same growth characteristics (fig. S3, B and C) with only minimal variations over 2 to 3 weeks of culture and were genetically diverse (fig. S3D). In addition, the cell mixture was genetically very similar to the parental line as detected by SKY (fig. S3E). Aliquots of this cell mixture were injected into multiple recipient mice and could then be followed in these mice by flow cytometry (Fig. 2B). We reasoned that preservation or a moderate reduction of intratumor heterogeneity in vivo should translate into a relatively equal repartition of the various colors. By contrast, loss of tumor diversity and emergence of one or a few dominant clones should strongly skew the color distribution (Fig. 2B). In addition, our strategy allows visualization of the spatial organization of individual cell progeny by means of intravital imaging (Fig. 2B). In sum, this multicolor labeling method offers the ability to gauge the extent of tumor heterogeneity in different anatomical locations, at different stages of tumor development, and under different experimental conditions.

Tumor heterogeneity is compartmentalized at the anatomical and microanatomical level

Upon transfer of a multicolor mix of tumor cells, we observed lymphoma growth primarily in the bone marrow but also in the spleen and in some lymph nodes—very similar to what is seen in Eμ-myc transgenic mice. We also occasionally observed tumor masses developing in nonlymphoid tissues, such as skin-associated nodules, a feature also observed in Eμ-myc mice (*13*). To assess whether the extent of tumor heterogeneity is similar across organs, we compared the color distribution in various organs of individual mice on day 21. As shown in Fig. 3A and fig. S4, we most often recovered the five colored lymphoma populations in the bone marrow, spleen, lymph nodes, and blood, although some degree of anatomical variations was noted in a given animal. Notably, tumor nodules developing in nonlymphoid compartments were almost always made of one colored population, suggestive of seeding from a single cell (Fig. 3A). Such restriction of diversity in nonlymphoid sites was also observed in $Rag^{-/-}$ mice, excluding a role for the adaptive immune response in these anatomical differences (fig. S5). For each sample, we calculated the evenness index (*16*), which reflects the diversity and abundance of the colored populations, with high (0.5 to 1) or low (<0.3) values reflecting balanced or strongly biased distribution, respectively (Fig. 3B). Overall, these results suggest that tumor cells maintain a degree of heterogeneity in lymphoid organs but not in nonlymphoid tumor nodules.

To better characterize how tumor heterogeneity is spatially organized in the bone marrow, the primary site of tumor development, we relied on intravital two-photon imaging. At early time points, we observed tumor seeding in the form of multiple small patches of cells, each composed of one color (Fig. 3C). Numerous patches of the different colors were detected in most of the areas imaged. In addition, time-lapse imaging revealed that tumor cells were largely sessile, consistent with the establishment of individual niches containing the progeny of one cell (movie S1). At later time points, patches became larger but remained largely nonoverlapping (Fig. 3C and movie S2). Overall, our results are consistent with a model in which numerous individual tumor cells establish their own niches in the bone marrow, providing a series of spatially compartmentalized locations for establishment of tumor diversity.

The immune response strongly affects tumor heterogeneity

We next assessed the potential role of the immune system in shaping intratumor heterogeneity. First, we tested the potential of T cells to attack lymphoma cells in the bone marrow. Intravital imaging of tumor-reactive activated T cells revealed efficient infiltration in the bone marrow

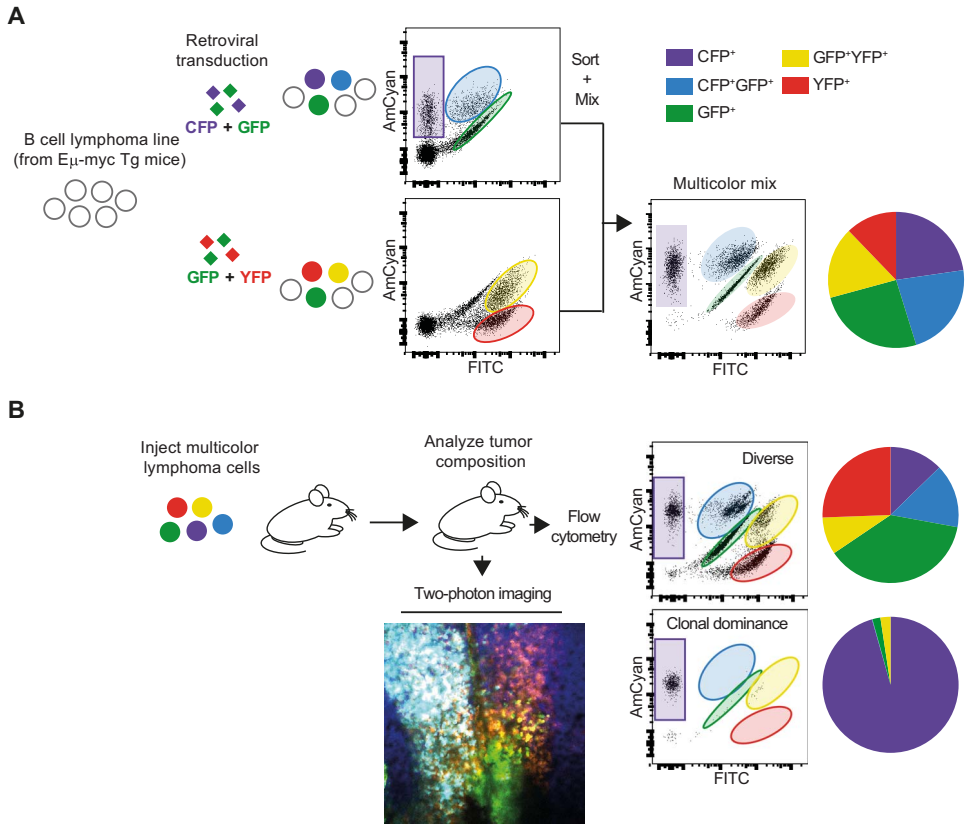

Fig. 2. A multicolor barcoding method to study intratumor clonal diversity. (**A**) Experimental setup used to produce color-barcoded tumors. Tumor cells isolated from a lymphoma-bearing Eμ-myc mouse were retrovirally transduced with a mixture of CFP- and GFP-encoding viruses or a mixture of GFP- and YFP-encoding viruses. CFP^+, GFP^+, YFP^+, CFP^+GFP^+, and GFP^+YFP^+ cells were sorted, and a mixture containing an equal proportion of each cell population was prepared. Tg, transgenic; FITC, fluorescein isothiocyanate. (**B**) Tracking intratumor heterogeneity using a multicolor labeling strategy. Multicolor-barcoded cells were injected in individual mice. At various time points, the tumor composition was analyzed by flow cytometry and/or intravital imaging of the bone marrow.

(Fig. 4, A and B), with some level of heterogeneity in T cell densities among individual clonal tumor patches. We frequently observed stable conjugates between T cells and lymphoma cells (Fig. 4C, movies S3 and S4, and fig. S6). These interactions were specific, because control T cells that are not tumor specific displayed higher motility and did not form stable contacts with tumor cells (Fig. 4, D and E; movie S5; and fig. S6). In addition, using a fluorescence resonance energy transfer (FRET) reporter for caspase 3 activation (*17*), we detected evidence for tumor apoptosis after contacts with tumor-reactive T cells (Fig. 4F and movies S6 and S7). As illustrated in Fig. 4 (A and B) and movie S3, patches with high T cell infiltration tended to contain fewer tumor cells, possibly as the result of T cell–mediated killing. These results suggest that B cell lymphomas can be efficiently infiltrated and attacked by cytotoxic $CD8^+$ T cells in the bone marrow.

One important consequence of intratumor heterogeneity is the potential variability in tumor antigen presentation. Tumor neoantigens may arise after the initial transformation event, leading to mosaic antigen expression. In addition, the frequent occurrence of chromosome loss could eliminate antigens from a fraction of the tumor cells, establishing a source of immune escape variants. To address how the immune system deals with intratumor diversity in the antigenic landscape, we took advantage of a male Eμ-myc tumor in which about 28% of the cells had lost the Y chromosome (Fig. 1C, lymphoma #1). We reasoned that, upon transfer into female recipients, H-Y should act as a tumor antigen in a subset of the lymphoma cells, mimicking a situation where only a fraction of the tumor cells is immunogenic. First, we observed that, whereas the tumor grew rapidly in male mice, female animals exhibited prolonged tumor control (Fig. 5A). This was somewhat surprising given the fact that a large fraction of the initial tumor cells had lost the Y chromosome and therefore should not be more immunogenic in females than in males. We then compared the extent of tumor diversity in the bone marrow of male versus female recipient mice using our multicolor coding strategy. We observed a drastic loss of tumor heterogeneity in female animals and the emergence of one (or a few) dominant clone(s) (Fig. 5, B to D). These results were confirmed by in situ imaging where tumor cell patches in female recipients typically consisted of one or two colors only (fig. S7). When tumors isolated from female recipients were cultured ex vivo to release the immune pressure, we did not observe re-emergence of new colors, suggesting a permanent sculpting (fig. S8). We also observed evidence for loss of tumor phenotypic diversity with unlabeled tumors in female mice (fig. S9), suggesting that immune-mediated restriction of tumor heterogeneity was not a consequence of the viral transduction used to label tumor cells. A kinetic analysis revealed that intratumor heterogeneity was initially high in both male and female but declined specifically in female recipients at later stages (Fig. 5, E and F). Restriction of diversity was not seen in male $Rag2^{-/-}$ or female $Rag2^{-/-}$ mice (Fig. 5F and fig. S10A), implicating adaptive immunity in this process. Moreover, the restriction was associated with the emergence of H-Y–specific $CD8^+$ T cells in female recipients and an overall higher frequency of interferon-γ (IFN-γ)–producing $CD8^+$ T cells in female recipients as compared with males (fig. S10, B to D). These results demonstrate that the adaptive immune response in female mice profoundly restricted tumor diversity over the course of the response.

Epitope spreading amplifies the impact of the immune response on tumor heterogeneity

To gain some insight into the mechanism underlying the shaping of tumor heterogeneity by the immune response, we analyzed the karyotype of the lymphoma cells developing in male or female mice. With respect to Y chromosome loss, we observed a similar frequency (28 to 48%) in the initial population (Fig. 1C, lymphoma #1) and after transfer in male mice (Fig. 6A), suggesting that tumor cells without Y chromosome proliferate on average at the same rate as the rest of the tumor population. In female animals, however, only cells without the Y chromosome were detected, demonstrating efficient elimination of all H-Y–expressing tumor cells (Fig. 6A), and this phenomenon required $CD8^+$ T cells (fig. S10E). It is, however, unlikely that the profound restriction

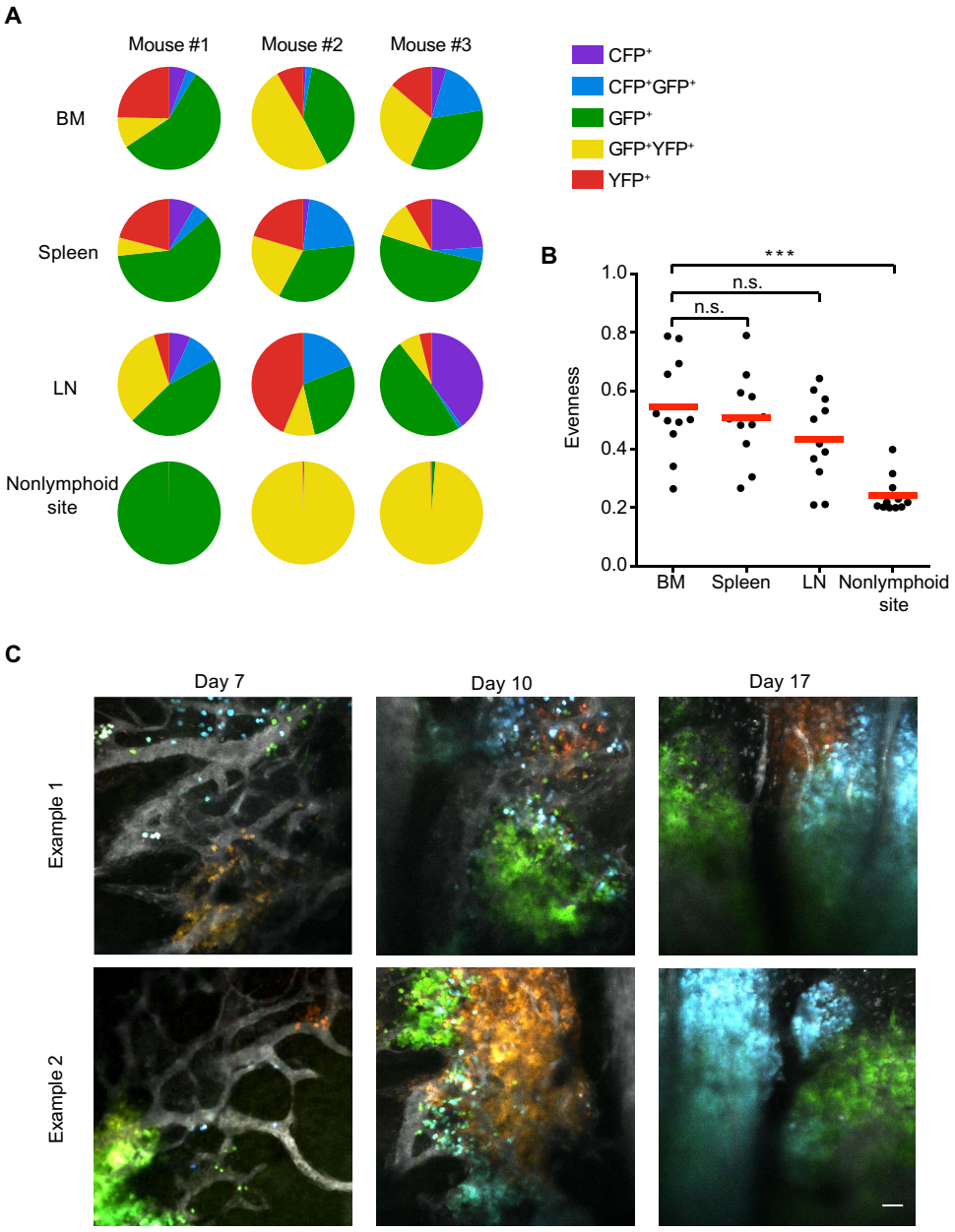

Fig. 3. Anatomical and microanatomical clonal heterogeneity in B cell lymphoma development. (**A**) Color-barcoded lymphoma B cells isolated from a male Eμ-myc transgenic mouse were injected intravenously into male recipients. Tumor cellular composition was analyzed 3 weeks later in the bone marrow (BM), spleen, lymph nodes (LN), and nonlymphoid sites of tumor growth. Pie charts show the distribution of individual colored tumors in the indicated organs for three representative animals. (**B**) The graph displays the evenness index measured in different organs for 11 individual mice. ***$P < 0.001$ (one-way ANOVA with Bonferroni's corrections). n.s., not significant. (**C**) Spatially organized architecture of clonal growth in the bone marrow. Color-barcoded tumor cells were injected intravenously, and recipients were subjected to intravital imaging of the bone marrow at the indicated time points. Two examples for each time points are shown and are representative of multiple regions of the bone marrow imaged in two independent experiments. Scale bar, 50 μm.

of tumor heterogeneity seen in female animals uniquely resulted from the elimination of H-Y–expressing tumor cells because around 1×10^5 cells (about 25% of injected cells) in the initial mix did not have the Y chromosome (Fig. 6A). Even when we restricted the analysis of these experiments to tumor cells that did not harbor the Y chromosome (X-only karyotypes), we observed a lower genetic diversity in females compared with males (Fig. 6A and fig. S11), with evidence of clonal dominance in females. This result suggested that the immune pressure exerted in female mice extended beyond H-Y–specific responses. We therefore explored the possibility that the anti–H-Y T cell response in female mice promoted a response to cryptic tumor antigens, a process often referred to as epitope spreading. Although the nature of tumor antigens expressed by our lymphoma line is not known, we took advantage of the introduction of the green fluorescent protein (GFP) and its variants in our multicolor tumor cell mix. The retroviral transduction of the fluorescent protein appears poorly immunogenic, and fluorescent cells are not eliminated in male mice. However, we observed that the tumor cells recovered from female animals displayed significantly lower fluorescence intensity than those recovered from male mice (Fig. 6, B and C). To confirm this finding, we injected a mixture of fluorescent and nonfluorescent tumor cells and again showed specific elimination of fluorescent tumors in female but not in male mice (Fig. 6D). This elimination was dependent on the endogenous T cell repertoire and was not simply a bystander effect of the anti–H-Y T cell response, because fluorescent cells were not specifically eliminated in female MataHari T cell receptor (TCR) transgenic mice in which all $CD8^+$ T cells are H-Y specific (Fig. 6D). We also excluded the possibility that female mice have an intrinsic higher capacity to mount anti-GFP responses (for example, due to a different preimmune TCR repertoire) compared with male animals (fig. S12). Last, we tested the presence of a $CD8^+$ T cell response against a previously defined H-$2D^b$–restricted epitope of GFP (*18*) and could detect a GFP-specific response in female but not in male animals (Fig. 6E). Together, our results support the idea that the immune system profoundly restricts intratumor heterogeneity of developing tumor cells even in the context of mosaic expression of a tumor antigen. This restriction occurred through the elimination of the most immunogenic cells and through broadening of the response to additional epitopes.

The immune response restricts intratumor genetic heterogeneity

To firmly establish that changes in intratumor diversity measured using fluorescent barcoding reflected changes at the genetic level, we relied on

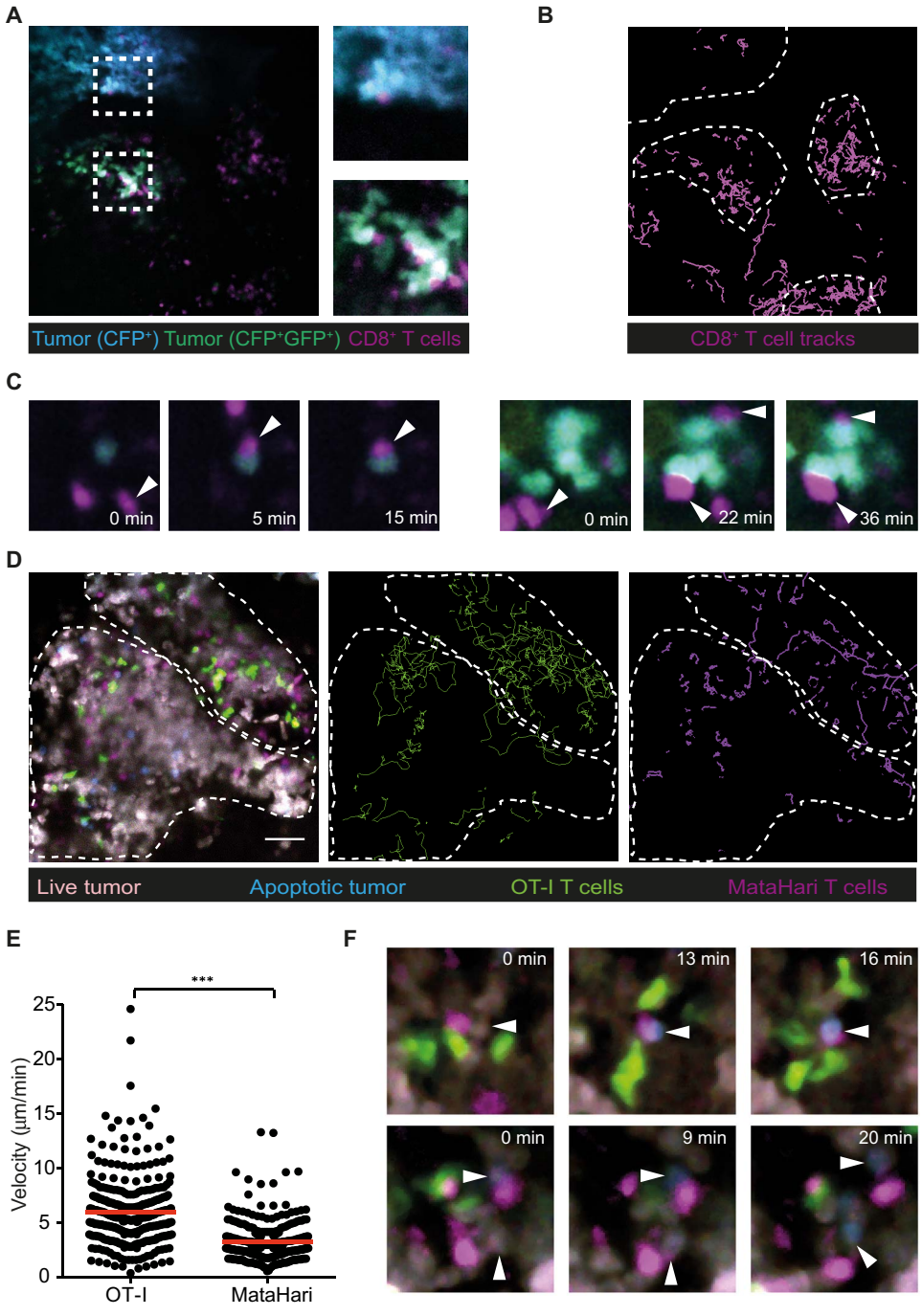

Fig. 4. CD8$^+$ T cells can infiltrate the bone marrow to form contacts with tumor cells. (**A** to **C**) Color-barcoded lymphoma B cells isolated from a male Eμ-myc transgenic mouse were injected intravenously into female recipients. On day 10, activated CD8$^+$ T cells bearing the anti–H-Y MataHari TCR were adoptively transferred. Intravital imaging of the bone marrow was performed 4 hours later. (A) Representative image showing CD8$^+$ T cell infiltration of colored tumor patches. Areas in the white square were enlarged to illustrate T cell–tumor cell interactions. Note that T cell infiltration in the different tumor patches showed a degree of heterogeneity. (B) CD8$^+$ T cells are preferentially confined within tumor patches. Tracks of CD8$^+$ T cells are shown in magenta, and tumor areas are delimited in white dashed lines. (C) Representative time-lapse images showing T cell–tumor cell encounters and subsequent establishment of stable cellular interactions. (**D** to **F**) Lymphoma B cells isolated from a male Eμ-myc transgenic mouse were transduced with a FRET-based reporter for caspase 3 activity and were injected intravenously into female recipients. On day 10, activated CD8$^+$ T cells bearing the anti–H-Y MataHari TCR (SNARF labeled) and similarly activated CD8$^+$ T cells from GFP-expressing OT-I TCR transgenic mice were adoptively transferred. Intravital imaging of the bone marrow was performed 4 hours later. (D) Left: Representative image showing MataHari T cells (magenta), OT-I T cells (green), live tumor cells (white), and apoptotic tumor cells (blue). Right: Tracks of individual MataHari and OT-I T cells are shown, illustrating a higher confinement for MataHari T cells. Scale bar, 50 μm. (E) Graph depicts velocities of individual OT-I and MataHari T cells (n = 352 and n = 295, respectively). Data are from two representative movies. ***P < 0.001 (unpaired t test). (F) Examples of tumor cells undergoing apoptosis after interactions with MataHari T cells.

tumor whole-exome sequencing. Of the relatively frequent mutations previously reported in Eμ-myc lymphoma (*19*), we identified mutations in *Trp53* in the tumor used. Several nonsynonymous mutations were predicted to generate putative neoantigens using the NetMHCpan algorithm (fig. S13) (*20*–*22*). For each identified single-nucleotide variant (SNV), we calculated its variant allele frequency (VAF). As described previously, the overall distribution of VAFs reflects the sample genetic heterogeneity. In clonal tumors, most SNVs should be present at a frequency of around 50% (that is, 50% of the reads harbor the mutation when the mutated allele is present in all cells), whereas the presence of multiple subclones in the sample implies that a large number of SNVs are present at low frequency (typically <20%). The mutant-allele tumor heterogeneity (MATH) score can be inferred from the VAF distribution to estimate intratumor genetic diversity (*23*, *24*). We first compared the genetic diversity in tumors growing in the bone marrow versus nonlymphoid sites (in the same recipients) because the diversity measured with fluorescent barcoding in these two locations was drastically different. Tumors isolated from the bone marrow were genetically more diverse as reflected by a high number of SNVs present at low frequency and a high MATH score. By contrast, tumor cells isolated from nonlymphoid sites

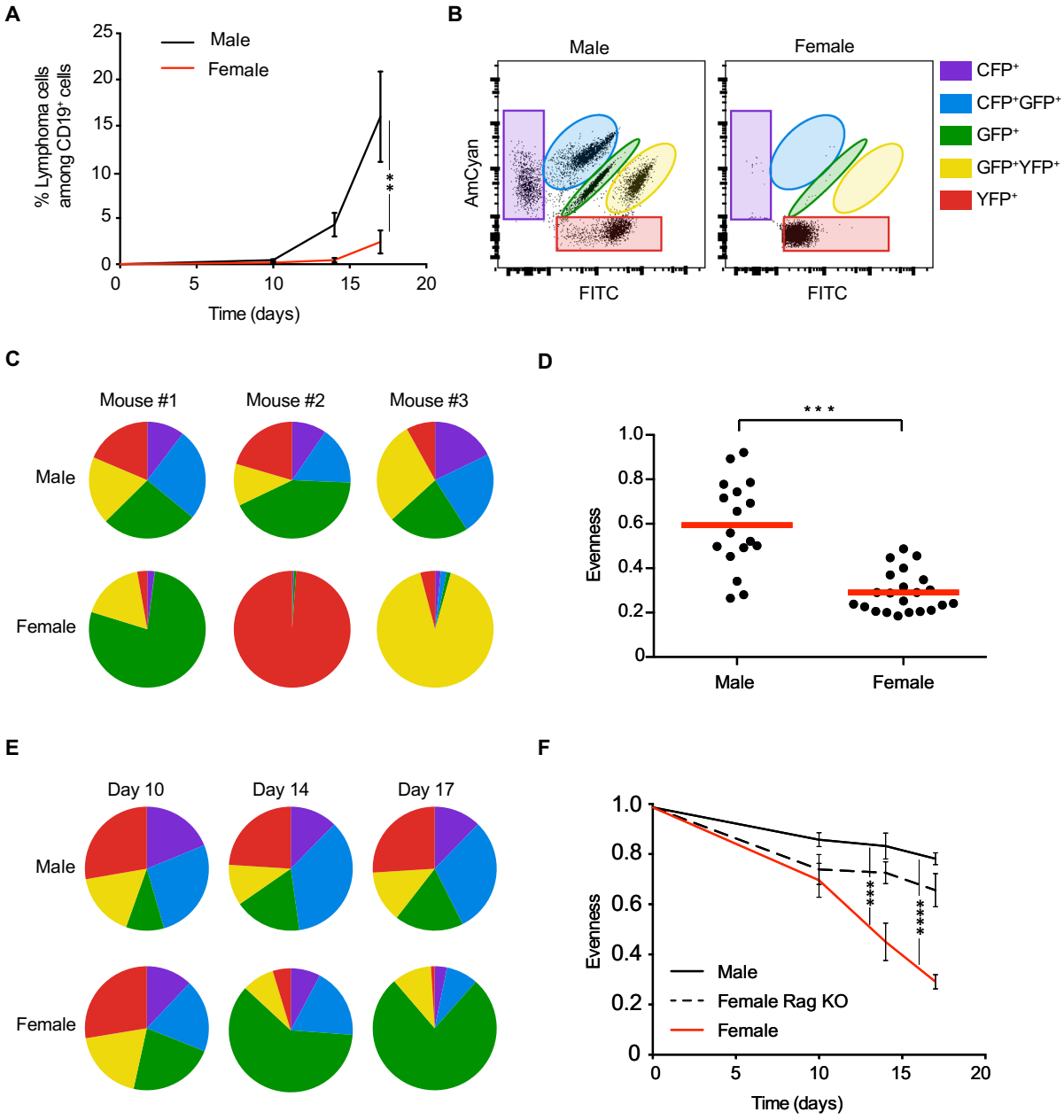

Fig. 5. The immune system strongly restricts tumor clonal heterogeneity. (**A** to **D**) Color-barcoded lymphoma B cells isolated from a male Eμ-myc transgenic mouse were injected intravenously into male or female recipients. (A) Tumor growth was monitored by measuring the percentage of tumor cells among total B cells in the blood at various time points. At least six mice were analyzed in each group. $^{**}P < 0.01$ (unpaired *t* test). (B) Female recipients display a highly reduced intratumoral clonal heterogeneity compared with their male counterparts. Representative flow cytometry plots showing the tumor cell composition retrieved from the bone marrow of a male or a female recipient at 3 weeks. (C) Pie charts representing the tumor composition in the bone marrow of three representative male and female recipients. (D) Graph shows the evenness index calculated from tumor cells retrieved at 3 weeks from the bone marrow of male ($n = 17$) or female ($n = 22$) recipients. Data are pooled from three independent experiments. $^{***}P < 0.001$ (unpaired *t* test). (**E** and **F**) Progressive decrease in tumor heterogeneity in female recipients. Longitudinal analysis of tumor composition analyzed in the blood of a representative male or female recipient. (F) Kinetic analysis of the evenness index for color-barcoded tumor injected in male, female, or female Rag2$^{-/-}$ (Rag2 KO) mice and recovered in the blood. At least six mice were analyzed for each group. $^{***}P < 0.001$ and $^{****}P < 0.0001$ (one-way ANOVA with Bonferroni's corrections).

had a low MATH score, with most SNV frequencies being close to 50% (Fig. 7, A and B). We further examined how the immune response was shaping intratumor genetic diversity by comparing VAF distributions in (male) tumor cells growing in male (low immune pressure) versus female (high immune pressure) recipients. We found that tumor cells isolated from female recipients had a significantly reduced intratumor genetic diversity, as shown by the VAF distributions and the calculated MATH scores (Fig. 7, C to E). In sum, these results confirm and extend our findings obtained with fluorescent barcoding, showing that the immune-mediated restriction of intratumor heterogeneity is apparent at the genetic level.

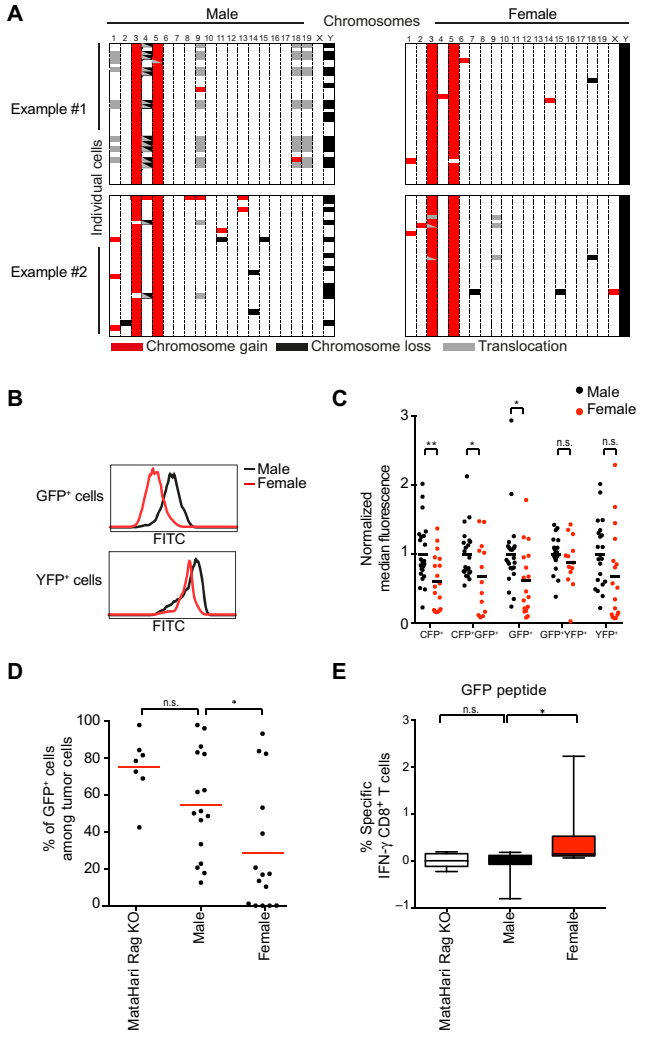

Fig. 6. Mechanisms of immune-mediated restriction of intratumor heterogeneity. (**A** to **C**) Color-barcoded lymphoma B cells isolated from a male Eμ-myc transgenic mouse (Fig. 1C, lymphoma #1) were injected intravenously into male or female recipients. The injected cell population and the tumor cells recovered from the bone marrow of male or female recipients were subjected to SKY or flow cytometry. (A) The immune response restricts the genetic diversity of tumor cells developing in female recipients. Tables recapitulating the karyotypes of 31 cells analyzed from the tumors of two male and two female recipients. Red represents gain of chromosomes, black represents loss of chromosomes, and gray shows translocations. (B) Fluorescence intensities were analyzed by flow cytometry. Representative histograms from one male and one female show the fluorescence intensities of the GFP^+ population (top) and YFP^+ population (bottom). (C) Graph shows normalized median fluorescence (FITC channel for all the populations except for the CFP^+ population for which AmCyan fluorescence is considered). The relative fluorescence is set to 1 for male recipients. Data are pooled from three independent experiments. $*P < 0.05$; $**P < 0.01$ (unpaired *t* test). A minimum of 18 mice were analyzed for each group. (**D**) Tumor cells expressing a fluorescent protein are eliminated in female but not in male mice. A mixture of fluorescent and unlabeled tumor cells was injected in male, female, or MataHari TCR transgenic $Rag2^{-/-}$ mice. After 3 weeks, tumors were isolated from the bone marrow, and the percentage of fluorescent tumor cells among tumor cells was analyzed by flow cytometry. Error bars represent SEM. Data are pooled from two independent experiments with a total of at least seven mice per group. $*P < 0.05$ (one-way ANOVA with Bonferroni's corrections). (**E**) $CD8^+$ T cells retrieved from the bone marrow of tumor-bearing recipients were restimulated for 4 hours with a GFP peptide (10 μM) in the presence of GolgiPlug and assayed for intracellular IFN-γ expression by flow cytometry. $*P < 0.05$ (one-way ANOVA).

Immune checkpoint inhibition restricts intratumor heterogeneity

We next asked whether immunotherapies aimed at increasing antitumor immune responses could also lead to the narrowing of tumor heterogeneity. We therefore treated male recipients injected with a male lymphoma with anti–PD-1 (programmed cell death protein 1) or anti–CTLA-4 (cytotoxic T lymphocyte–associated antigen 4). In this model, the effect of checkpoint blockade did not strongly affect tumor growth, with a transient reduction of tumor load upon anti–PD-1 treatment (fig. S14, A and B). Nevertheless, anti–PD-1 treatment significantly reduced tumor diversity and favored clonal dominance (Fig. 8, A and B). No significant effect was detected for anti–CTLA-4. To maximize the effect, we repeated the experiments using a combination of anti–PD-1 and anti–CTLA-4 antibody (Ab), a treatment that induced a modest increase (median survival from 19 to 26 days) in survival in tumor-bearing mice (fig. S14C). In these settings also, checkpoint blockade significantly decreased intratumor heterogeneity (Fig. 8C). This was likely due to a broadening of the antitumor immune response, given that we detected evidence for a response against the GFP specifically in treated mice (Fig. 8D). Tumors emerging in mice treated with anti–PD-1 and anti–CTLA-4 and retransferred in secondary recipients lost the modest response to checkpoint inhibitors, suggesting that clonal dominance was associated with tumor immunoediting (fig. S15). To extend these findings to a different B cell tumor model, we used viral-Abelson kinase (v-abl)–transformed pro-B cells (*25*, *26*). One advantage of this approach is that transformed B cells are generated in vitro and thus have not been subjected to any immunoediting. Combined anti–PD-1 and anti–CTLA-4 treatment had a modest effect on tumor growth (fig. S14D), associated with an increased infiltration of $CD8^+$ T cells (Fig. 8E). Our multicolor labeling strategy also revealed a decrease in tumor heterogeneity upon checkpoint blockade (Fig. 8F). Thus, immune checkpoint inhibitors can shape the fine tumor composition and restrict its diversity even in the absence of strong control of tumor growth.

DISCUSSION

Individual tumors most often display extensive heterogeneity, in part fueled by genomic instability. Although many studies have explored how immune effectors limit tumor growth, we critically lack information on the impact of the immune response on the subclonal composition of tumors. Analyzing B cell lymphomas spontaneously developing in Eμ-myc transgenic mice, we noted extensive aneuploidy and a large intratumor genetic diversity. In particular, we observed many cells lacking one or several chromosomes. Because this phenomenon may result in the potential loss of tumor neoantigens, it is therefore tempting to consider that these cells constitute a reservoir for immune escape. In support of this idea, we have shown the outgrowth of tumor cells that have lost the Y chromosome when lymphoma cells were injected in female mice. Although further work will be needed to evaluate the contribution of chromosome loss to immune escape, a recent study correlated elevated tumor aneuploidy to a lower level of cytotoxic immune cells in human cancer patients (*27*).

To tackle tumor diversity in a model of MYC-driven B cell lymphoma, we introduced a multicolor barcoding strategy. Our method complements genetic barcoding (*28*, *29*), other fluorescent labeling approaches (*14*, *15*), or lineage tracing strategies (*30*–*33*) with specific advantages. First, our fluorescent barcoding is adapted to flow cytometry with the possibility of tracking five distinct populations: This was sufficient to detect the emergence of a dominant clone and to compare

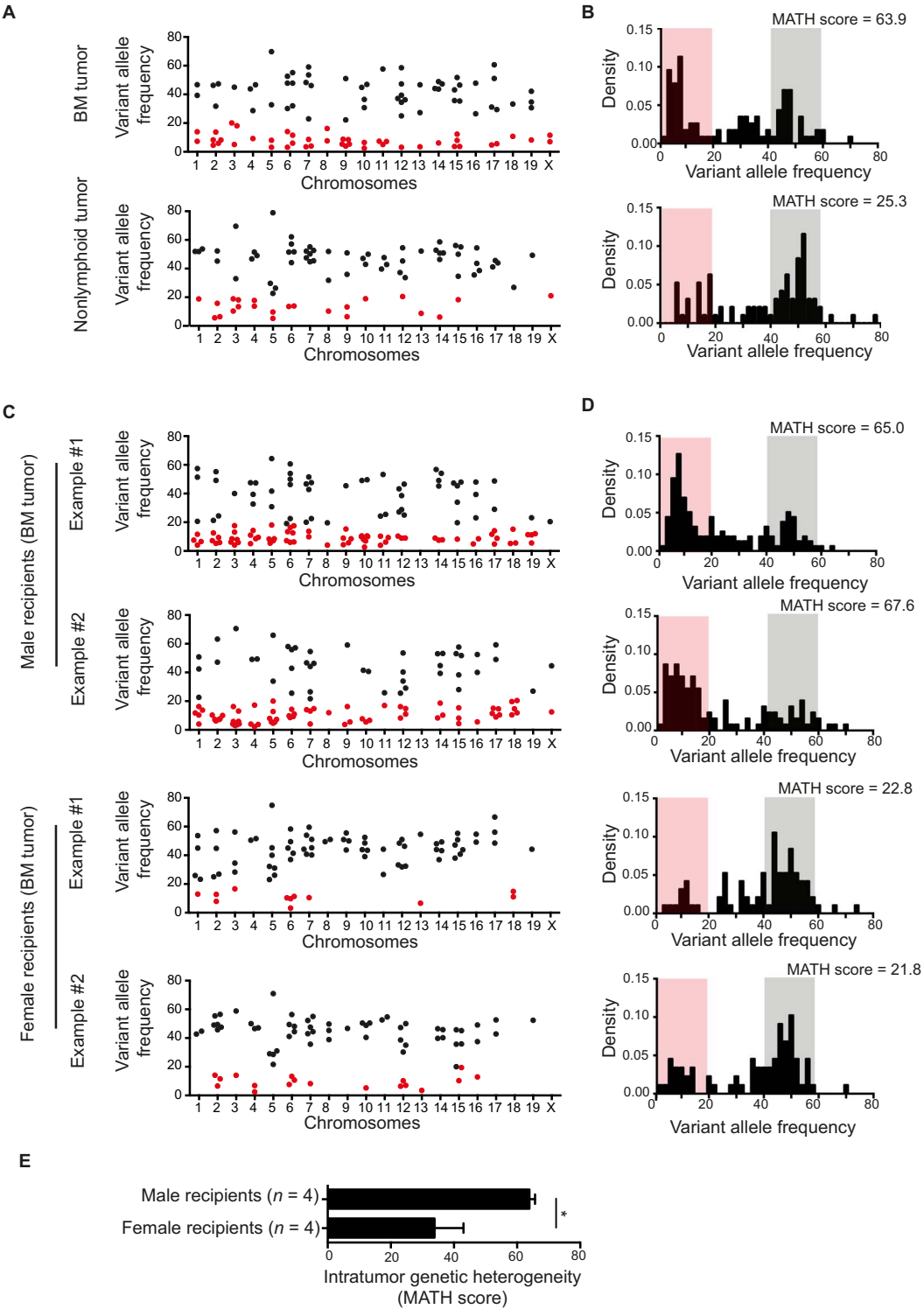

Fig. 7. The immune system strongly restricts tumor genetic heterogeneity. Lymphoma B cells isolated from a male Eμ-myc transgenic mouse were injected intravenously into male or female recipients. Tumor cells recovered from the bone marrow or nonlymphoid sites of male or female recipients were subjected to whole-exome sequencing. (**A** and **B**) Higher intratumor genetic heterogeneity in tumors developing in the bone marrow as compared with nonlymphoid site in the same male animal. (A) The VAF for each SNV is shown with the corresponding chromosome. SNVs with VAFs <20% are highlighted in red. (B) Graph shows the density distribution of VAFs. (**C** to **E**) Higher intratumor genetic heterogeneity in tumors developing in male compared with female recipients. (C) Whole-exome sequencing was performed on eight tumor samples (recovered from the bone marrow of four male and four female recipients). For two representative tumors of each group, the VAF for each SNV is shown with the corresponding chromosome. SNVs with VAFs <20% are highlighted in red. (D) Graphs show the density distribution of VAFs. (E) After whole-exome sequencing, the MATH score was used to evaluate intratumor heterogeneity in tumors recovered from male ($n = 4$) and female ($n = 4$) recipients. *$P < 0.05$ (unpaired t test)

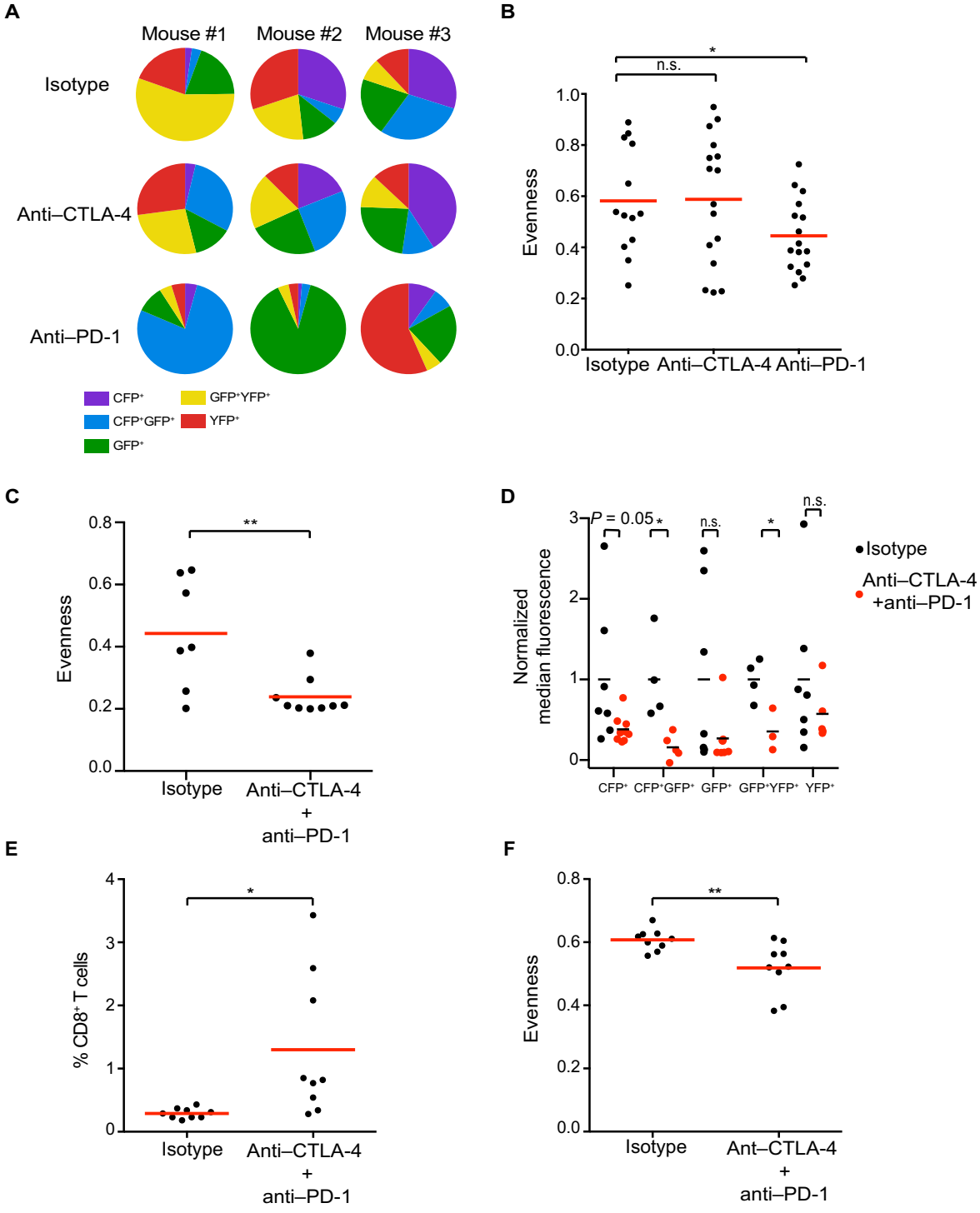

Fig. 8. Immune checkpoint inhibition reduces intratumor heterogeneity. (**A** to **D**) Lymphoma B cells isolated from a male Eμ-myc transgenic mouse were injected intravenously into male recipients. Recipients were injected every 3 days with the indicated Abs. (A) Pie charts representing the tumor composition in the bone marrow of three representative mice from each group at 3 weeks. (B) Graph shows the evenness index calculated from tumor cells retrieved at 3 weeks from the bone marrow of individual mice. Each dot represents one animal. Data are compiled from two independent experiments with at least 13 mice per group. *$P < 0.05$ (unpaired *t* test). (C) Combined anti–PD-1 and anti–CTLA-4 treatment reduces tumor diversity. Graph shows the evenness index calculated from bone marrow tumor cells for the indicated group. Each dot represents one animal. **$P < 0.01$ (unpaired *t* test). (D) Graph shows normalized median fluorescence (FITC channel for all the populations except for the CFP^+ population for which AmCyan fluorescence is considered). The relative fluorescence is set to 1 for isotype-treated recipients. *$P < 0.05$ (unpaired *t* test). (**E** and **F**) v-abl–transformed pro-B cells from female mice were injected intravenously into female recipients. Recipients were injected every 3 days with the indicated Abs. (E) Graph shows percentage of $CD8^+$ T cells present in the bone marrow at 2 weeks after tumor injection. Each dot represents one animal. *$P < 0.05$ (unpaired *t* test). (F) Graph shows the evenness index calculated for tumor cells in the bone marrow at 2 weeks. Each dot represents an individual mouse. **$P < 0.01$ (unpaired *t* test).

tumor composition in different locations and could be used to assess phenotypic variations within distinct tumor subsets. Second, this approach can be combined with intravital imaging, offering insight into tumor motility and growth. In our lymphoma model, we found that individual tumor subclones seeding the bone marrow established their own compartmentalized niche, an architecture likely favored by their low motility. Thus, the progenies of different subclones appear spatially separated at the microanatomical level, with potential variability in the access to therapeutic drugs and/or to the immune infiltrate. Evidence for spatially separated subclones has been provided in human cancer patients by sampling of multiple tumor regions (*3*, *34*).

A key unanswered question in cancer development is the relationship between intratumoral heterogeneity and the ongoing immune response. We used tumor cells derived from a male mouse in which a fraction of tumor cells has lost the Y chromosome to mimic heterogeneity in tumor antigen expression. We found that, upon transfer into females but not into males, tumor diversity was lost and one dominant clone typically emerged. At least two phenomena concurred to restrict tumor diversity. First, we observed the efficient elimination of all tumor cells harboring the Y chromosome, most likely because of their high immunogenicity. Second, our results support the idea that the immune response in female mice extended to subdominant or cryptic epitopes, a process referred to as epitope spreading. This was illustrated by the elimination of tumor cells expressing high levels of fluorescent proteins and the detection of GFP-specific $CD8^+$ T cell responses specifically in female recipients. We speculate that the T cell responses also extend to other unknown subdominant tumor antigens. Epitope spreading has been described in a variety of contexts including autoimmunity (*35*). With respect to cancer, vaccination of melanoma patients against MAGE antigens has been shown to elicit CTLs directed against tumor antigens not harbored by the vaccine (*36*, *37*). We propose that epitope spreading represents an important mechanism by which the immune system narrows tumor diversity. The model of immunoediting postulates that the immune pressure will lead to the emergence of escape variants (*7*). This has been elegantly demonstrated through the observation that tumor cells lacking immunogenic neoantigens emerged as a result of T cell–mediated pressure (*38*, *39*). Evidence for tumor immunoediting has also been provided in human patients (*40*, *41*). However, most previous analyses of tumor immunoediting have not been performed at the clonal level and therefore have not directly addressed whether reduced tumor antigenicity promoted by the immune pressure originates from substantial changes in intratumor clonal diversity. Our results are consistent with a progressive narrowing of tumor diversity at the clonal and genomic levels and suggest that a single subclone may emerge as a consequence of an efficient immune response. Such a subclone may have preexisted at low frequency at early stages, in a process that would be very similar to what is observed during tumor escape from conventional therapy (*28*, *42*–*44*). Alternatively, immune escape could appear later during an equilibrium phase with the immune response. In this context, it has been recently proposed that T cell–derived IFN-γ could increase genetic instability in tumor cells and favor immunoediting (*9*).

We also analyzed the effect of checkpoint blockade on tumor heterogeneity. We found that anti–PD-1 treatment significantly decreased intratumor diversity even in models in which the effect on tumor burden was limited. Recent analyses of acquired resistance to PD-1 blockade in patients with metastatic melanoma revealed the outgrowth of cells with defects in IFN receptor signaling or in antigen presentation (*45*). Together, these results support a model in which the increased immune pressure mediated by anti–PD-1 leads to the elimination of most subclones, restricting overall heterogeneity and favoring clonal dominance. Such diminished intratumor clonal heterogeneity could also account for the reduced mutational burden recently observed in melanoma patients treated with anti–PD-1 (*46*). Whether tumors with a reduced genetic complexity could be more easily targeted through secondary therapies will be important to assess, in particular to define the best settings for drug combinations. A recent study in human cancer patients has reported an inverse association between the level of intratumor heterogeneity and the extent of immune infiltration (*47*). Our results may provide a causal link for these correlations by showing that a low level of intratumor heterogeneity arises as a result of a strong antitumor immune reaction. Future work using slowly developing spontaneous tumors and additional cancer models will be important to generalize this idea.

By using a multicolor tumor barcoding to track the spatiotemporal dynamics of tumor diversity as well as whole-exome sequencing, we revealed that the immune response can profoundly restrict intratumor clonal and genetic heterogeneity in a developing lymphoma, a process favored by the phenomenon of epitope spreading. Understanding how specific immunotherapies not only control tumor burden but also alter the overall intratumor heterogeneity represents an important goal to guide and optimize treatment strategies.

MATERIALS AND METHODS

Study design

The aim of this study was to establish the impact of the immune response on tumor heterogeneity. For this, we fluorescently barcoded lymphoma cells and transferred them in recipients subjected to different intensities of immune pressure. Tumor heterogeneity was assessed using a combination of intravital imaging in the bone marrow, flow cytometry, SKY, and whole-exome sequencing. Two models of B cell lymphoma were used, and treatment with anti–PD-1 and anti–CTLA-4 was evaluated. The number of mice per experimental group and the number of repetitions of the experiments are indicated in individual figure legends.

Mice

C57BL/6 (B6) mice were purchased from Charles River Laboratories. Eμ-myc transgenic, MataHari TCR transgenic (*48*), $Rag2^{-/-}$, and CD45.1 B6 mice were bred in our animal facility. All mice used were 8 to 12 weeks old. All procedures were performed in agreement with the Pasteur Institute's institutional guidelines for animal care. Experimental protocols were approved by the Animal Ethics Committee #1 of the Comité Régional d'Ethique pour l'Expérimentation Animale, Ile de France.

Flow cytometry

Cells were stained with the following Abs: allophycocyanin (APC)–eFluor 780–conjugated anti-CD8a (clone 53.67; catalog no. 47-0081-82), Alexa Fluor 647–conjugated anti–IFN-γ (XMG1.2; catalog no. 51-7311-82) (eBioscience), phycoerythrin (PE)–Cy7–conjugated anti-CD19 (6D5; catalog no. 115520), biotinylated anti-CD45.1 (A20; catalog no. 110704), and PE- or Alexa Fluor 647–conjugated streptavidin (catalog nos. 405204 and 405237, respectively) (BioLegend). Intracellular IFN-γ staining was performed using the Cytofix/Cytoperm Kit (BD Biosciences) according to the manufacturer's instructions. Before IFN-γ staining, cells were restimulated for 4 hours with 10 μM $GFP_{118–126}$ peptide (DTLVNRIEL, CliniSciences) in the presence of

GolgiPlug (BD Biosciences). Flow cytometry was performed on a FACSCanto II or an LSR/Fortessa cytometer (BD Biosciences) and analyzed using FlowJo software v.10.0.6 (Tree Star). Cell sorting was performed on an Aria III sorter (BD Biosciences).

Spectral karyotyping

Metaphases were prepared as described (*49*). Briefly, cells were incubated with colcemid (0.03 μg/ml; KaryoMAX Colcemid Solution, Life Technologies) for 3 hours at 37°C. Cells were then incubated in 0.075 M KCl for 10 min at 37°C, fixed (75% methanol/25% acetic acid), and washed three times in the fixative solution. Cell suspensions were dropped onto humid slides, which were air dried for further analysis. SKY was performed on metaphases using the mouse chromosome sky probe (MetaSystems) according to the manufacturer's instructions. Metaphases were imaged using a ZEISS AxioImager.Z2 microscope and a Metafer automated capture system (MetaSystems). At least 20 metaphases were analyzed for each sample.

Multicolor barcoding of tumor cells

Lymphoma cell lines were isolated from tumor-bearing female or male Eμ-myc mice (*13*), a transgenic mouse developing spontaneous Burkitt-like lymphomas. Immortalized pro-B cell lines were generated by infecting bone marrow cells with a retrovirus encoding v-abl (*26*, *49*, *50*). To produce viruses encoding fluorescent proteins, the following vectors were used: pMSCV-eCFP-N1, pMSCV-eGFP-N3, and pMSCV-eYFP-N1. Eμ-myc B cell lymphoma or transformed pro-B cells (3×10^6) were incubated with medium containing a mixture of CFP (cyan fluorescent protein)– and GFP-encoding retroviral particles or a mixture of GFP- and YFP (yellow fluorescent protein)–encoding retroviral particles for spin transduction in the presence of polybrene (8 μg/ml; Sigma-Aldrich). Cells were sorted 2 days later to isolate five distinct populations (CFP^+, GFP^+, YFP^+, CFP^+GFP^+, and GFP^+YFP^+). Sorted cells were mixed at an equivalent ratio and expanded, and the multicolor mix was intravenously injected (5×10^5 cells) in the indicated recipients. To quantify intratumor diversity, we used the evenness index. Evenness is based on Simpson's diversity index, which is commonly used in ecology to describe the diversity and abundance of species within a habitat (*16*). Evenness index was calculated according to the following formula:

$$\left[\sum_{i=1}^{5}(c_i)^2\right]^{-1} \times \frac{1}{5}$$, where C_i represents the fraction of the tumor population i (among total tumor cells) detected in the indicated organ.

Intravital two-photon imaging of the bone marrow

Bone marrow imaging was performed by adapting a previously described protocol (*51*) and using an upright microscope (DM6000 B, Leica) with a water-dipping 25×/1.05 numerical aperture objective (Olympus). Excitation was provided with a Ti:sapphire laser (Coherent) tuned at 880 to 920 nm. Mice were anesthetized with a mixture of xylazine (Rompun, 10 mg/kg) and ketamine (Imalgène, 100 mg/kg), which was replenished hourly. The scalp hair was removed, and the scalp was incised at the midline. The skull was then exposed, and a small steel plate with a cut-through hole was centered above the frontoparietal suture, glued to the skull using a cyanoacrylate-based glue, and bolted down. To visualize blood vessels, mice were injected intravenously with 200 μg of Evans blue (Sigma-Aldrich). During imaging, mice were supplied with oxygen and their core temperature was maintained at 37°C. To create time-lapse sequences, we typically scanned a 50-μm-thick volume of tissue at 5-μm Z steps and 30-s intervals. Three-dimensional (3D) cell tracking was performed using Imaris software (Bitplane). Movies and figures based on two-photon microscopy are shown as 2D maximum intensity projections of 3D data. The following filters were used: 483/32 (CFP), 520/35 (GFP), 542/27 (YFP), and 641/75 (Evans blue). To represent the various colors, YFP was pseudocolored in red.

T cell adoptive transfer and checkpoint blockade

Splenocytes from MataHari TCR transgenic mice were cultured for 2 days in the presence of H-$2D^b$–restricted $Uty_{246–254}$ peptide (WMHHNMLDI). Cells were then subjected to Ficoll gradient centrifugation and cultured with complete medium containing human interleukin-2 (20 ng/ml; ROCKLAND). Cells were used on days 4 to 8, at which time >95% were $CD8^+$ T cells. Cells were stained with 10 μM SNARF-1 (Life Technologies) and adoptively transferred into tumor-bearing mice. Intravital imaging was started 4 hours after transfer. To test the effects of checkpoint blockade, we intravenously injected 250 μg of anti–PD-1 (RMP1-14, Bio X Cell) or 250 μg of anti–CTLA-4 (9H10, Bio X Cell) every 3 days. A control group was injected with 250 μg of rat immunoglobulin G2a (IgG2a) isotype control (2A3, Bio X Cell) or polyclonal Syrian hamster IgG (Bio X Cell).

Whole-exome sequencing

Whole-exome sequencing was performed on tumor cells recovered from the bone marrow or from nonlymphoid sites of the indicated recipient mice (New York Genome Center). Libraries were prepared using the Agilent SureSelectXT Target Enrichment System in accordance with the manufacturer's instructions. Briefly, 200 ng of DNA was sheared using a Covaris LE220 sonicator (adaptive focused acoustics). DNA fragments were end repaired, adenylated, ligated to Illumina sequencing adapters, and amplified by polymerase chain reaction (PCR) (using 10 cycles). Exome capture was subsequently performed using 500 to 750 ng of the DNA library and the Agilent SureSelectXT Mouse All Exon Capture Probe Set (version 1). Captured exome libraries were then enriched by PCR (using 10 cycles). Final libraries were evaluated using fluorescent-based assays including PicoGreen (Life Technologies) or Qubit Fluorometer (Invitrogen) and Fragment Analyzer (Advanced Analytics) or BioAnalyzer (Agilent 2100) and were sequenced on an Illumina HiSeq 2500 sequencer (v4 chemistry; v2 chemistry for Rapid Run) using 2 × 125–base pair cycles and aiming for a coverage of 150×. Actual coverage ranged from 110× to 150×. SNVs were called by MuTect, Strelka, and LoFreq, and the corresponding VAF was calculated. To estimate intratumor diversity, we used the MATH score that corresponds to the ratio of the width to the center of the distribution of VAFs. Specifically, the MATH score was calculated from the median absolute deviation (MAD) and the median of the VAF distribution as MATH = 100*MAD/median, as described in (*23*, *24*). Typically, high intratumor heterogeneity is reflected by a wider distribution of VAFs with numerous SNVs present at low frequency (typically <20%) and therefore a high MATH score. Highly homogeneous (clonal) tumors contain primarily SNVs with VAFs of about 50% and display a low MATH score.

Statistical analysis

Significance was assessed by Student's *t* test or one-way analysis of variance (ANOVA), as specified in individual figure legends. Points in graphs indicate individual mice, and lines indicate means. In bar graphs, bars indicate means, and error bars indicate SEM. Analysis was performed using GraphPad Prism software.

SUPPLEMENTARY MATERIALS

immunology.sciencemag.org/cgi/content/full/3/29/eaat1435/DC1

Fig. S1. Lymphoma B cells developing in Eμ-myc transgenic mice display extensive intratumor genetic diversity.
Fig. S2. Frequent chromosome loss in MYC-driven lymphoma B cells.
Fig. S3. Multicolor fluorescently labeled tumor cells maintain clonal and genomic heterogeneity.
Fig. S4. Tumor heterogeneity is also detected in the blood.
Fig. S5. Tumor clonal dominance in nonlymphoid sites is independent of the adaptive immune system.
Fig. S6. Tumor-specific $CD8^+$ T cells form long-lasting contacts with tumor cells in the bone marrow.
Fig. S7. Restricted tumor diversity in female recipients as detected by intravital imaging.
Fig. S8. The immune-mediated restriction of intratumor heterogeneity is not reversible upon in vitro culture.
Fig. S9. Untransduced lymphoma cells exhibit higher phenotypic diversity in males compared with females.
Fig. S10. The restriction of tumor heterogeneity requires the adaptive immune system with an important role for $CD8^+$ T cells.
Fig. S11. Lymphoma cells with an X-only karyotype are less diverse in females compared with males.
Fig. S12. GFP is not more immunogenic in female than in male mice.
Fig. S13. Putative neoantigens in Eμ-myc tumors.
Fig. S14. Modest reduction in tumor load upon checkpoint blockade.
Fig. S15. Restriction of tumor diversity mediated by checkpoint blockade is associated with tumor immunoediting.
Movies S1 and S2. Lymphoma subclones establish independent niches in the bone marrow.
Movie S3. $CD8^+$ T cells infiltrate the bone marrow and interact with lymphoma cells.
Movie S4. $CD8^+$ T cells form stable contacts with lymphoma cells.
Movie S5. Tumor-reactive but not control $CD8^+$ T cells establish stable contacts with tumor cells in the bone marrow.
Movie S6. Visualization of lymphoma cell apoptosis after interactions with tumor-reactive $CD8^+$ T cells.
Movie S7. Lymphoma cell apoptosis after interactions with tumor-reactive $CD8^+$ T cells but not control T cells.
Table S1. Raw datasets.

REFERENCES AND NOTES

1. P. C. Nowell, The clonal evolution of tumor cell populations. *Science* **194**, 23–28 (1976).
2. L. M. Merlo, J. W. Pepper, B. J. Reid, C. C. Maley, Cancer as an evolutionary and ecological process. *Nat. Rev. Cancer* **6**, 924–935 (2006).
3. M. Gerlinger, A. J. Rowan, S. Horswell, J. Larkin, D. Endesfelder, E. Gronroos, P. Martinez, N. Matthews, A. Stewart, P. Tarpey, I. Varela, B. Phillimore, S. Begum, N. Q. McDonald, A. Butler, D. Jones, K. Raine, C. Latimer, C. R. Santos, M. Nohadani, A. C. Eklund, B. Spencer-Dene, G. Clark, L. Pickering, G. Stamp, M. Gore, Z. Szallasi, J. Downward, P. A. Futreal, C. Swanton, Intratumor heterogeneity and branched evolution revealed by multiregion sequencing. *N. Engl. J. Med.* **366**, 883–892 (2012).
4. A. Marusyk, V. Almendro, K. Polyak, Intra-tumour heterogeneity: A looking glass for cancer? *Nat. Rev. Cancer* **12**, 323–334 (2012).
5. E. M. F. De Sousa, L. Vermeulen, E. Fessler, J. P. Medema, Cancer heterogeneity—A multifaceted view. *EMBO Rep.* **14**, 686–695 (2013).
6. R. A. Burrell, N. McGranahan, J. Bartek, C. Swanton, The causes and consequences of genetic heterogeneity in cancer evolution. *Nature* **501**, 338–345 (2013).
7. R. D. Schreiber, L. J. Old, M. J. Smyth, Cancer immunoediting: Integrating immunity's roles in cancer suppression and promotion. *Science* **331**, 1565–1570 (2011).
8. D. Mittal, M. M. Gubin, R. D. Schreiber, M. J. Smyth, New insights into cancer immunoediting and its three component phases—Elimination, equilibrium and escape. *Curr. Opin. Immunol.* **27**, 16–25 (2014).
9. K. Takeda, M. Nakayama, Y. Hayakawa, Y. Kojima, H. Ikeda, N. Imai, K. Ogasawara, K. Okumura, D. M. Thomas, M. J. Smyth, IFN-γ is required for cytotoxic T cell-dependent cancer genome immunoediting. *Nat. Commun.* **8**, 14607 (2017).
10. A. Woloszynska-Read, P. Mhawech-Fauceglia, J. Yu, K. Odunsi, A. R. Karpf, Intertumor and intratumor NY-ESO-1 expression heterogeneity is associated with promoter-specific and global DNA methylation status in ovarian cancer. *Clin. Cancer Res.* **14**, 3283–3290 (2008).
11. A. A. Jungbluth, E. Stockert, Y. T. Chen, D. Kolb, K. Iversen, K. Coplan, B. Williamson, N. Altorki, K. J. Busam, L. J. Old, Monoclonal antibody MA454 reveals a heterogeneous expression pattern of MAGE-1 antigen in formalin-fixed paraffin embedded lung tumours. *Br. J. Cancer* **83**, 493–497 (2000).
12. N. McGranahan, A. J. Furness, R. Rosenthal, S. Ramskov, R. Lyngaa, S. K. Saini, M. Jamal-Hanjani, G. A. Wilson, N. J. Birkbak, C. T. Hiley, T. B. Watkins, S. R. Shafi, N. Murugaesu, R. Mitter, A. U. Akarca, J. Linares, T. Marafioti, J. Y. Henry, E. M. Van Allen, D. Miao, B. Schilling, D. Schadendorf, L. A. Garraway, V. Makarov, N. A. Rizvi, A. Snyder, M. D. Hellmann, T. Merghoub, J. D. Wolchok, S. A. Shukla, C. J. Wu, K. S. Peggs, T. A. Chan, S. R. Hadrup, S. A. Quezada, C. Swanton, Clonal neoantigens elicit T cell immunoreactivity and sensitivity to immune checkpoint blockade. *Science* **351**, 1463–1469 (2016).
13. A. W. Harris, C. A. Pinkert, M. Crawford, W. Y. Langdon, R. L. Brinster, J. M. Adams, The E mu-myc transgenic mouse. A model for high-incidence spontaneous lymphoma and leukemia of early B cells. *J. Exp. Med.* **167**, 353–371 (1988).
14. K. Weber, M. Thomaschewski, M. Warlich, T. Volz, K. Cornils, B. Niebuhr, M. Täger, M. Lütgehetmann, J. M. Pollok, C. Stocking, M. Dandri, D. Benten, B. Fehse, RGB marking facilitates multicolor clonal cell tracking. *Nat. Med.* **17**, 504–509 (2011).
15. M. Mohme, C. L. Maire, K. Riecken, S. Zapf, T. Aranyossy, M. Westphal, K. Lamszus, B. Fehse, Optical barcoding for single-clone tracking to study tumor heterogeneity. *Mol. Ther.* **25**, 621–633 (2017).
16. H. Wu, J. Carrillo, J. Ding, Species diversity and environmental determinants of aquatic and terrestrial communities invaded by *Alternanthera philoxeroides*. *Sci. Total Environ.* **581–582**, 666–675 (2017).
17. B. Breart, F. Lemaitre, S. Celli, P. Bousso, Two-photon imaging of intratumoral $CD8^+$ T cell cytotoxic activity during adoptive T cell therapy in mice. *J. Clin. Invest.* **118**, 1390–1397 (2008).
18. W. G. Han, W. W. Unger, M. H. Wauben, Identification of the immunodominant CTL epitope of EGFP in C57BL/6 mice. *Gene Ther.* **15**, 700–701 (2008).
19. M. Lefebure, R. W. Tothill, E. Kruse, E. D. Hawkins, J. Shortt, G. M. Matthews, G. P. Gregory, B. P. Martin, M. J. Kelly, I. Todorovski, M. A. Doyle, R. Lupat, J. Li, J. Schroeder, M. Wall, S. Craig, G. Poortinga, D. Cameron, M. Bywater, L. Kats, M. D. Gearhart, V. J. Bardwell, R. A. Dickins, R. D. Hannan, A. T. Papenfuss, R. W. Johnstone, Genomic characterisation of Eμ-Myc mouse lymphomas identifies Bcor as a Myc co-operative tumour-suppressor gene. *Nat. Commun.* **8**, 14581 (2017).
20. I. Hoof, B. Peters, J. Sidney, L. E. Pedersen, A. Sette, O. Lund, S. Buus, M. Nielsen, NetMHCpan, a method for MHC class I binding prediction beyond humans. *Immunogenetics* **61**, 1–13 (2009).
21. M. Nielsen, M. Andreatta, NetMHCpan-3.0; improved prediction of binding to MHC class I molecules integrating information from multiple receptor and peptide length datasets. *Genome Med.* **8**, 33 (2016).
22. V. Jurtz, S. Paul, M. Andreatta, P. Marcatili, B. Peters, M. Nielsen, NetMHCpan-4.0: Improved peptide-MHC class I interaction predictions integrating eluted ligand and peptide binding affinity data. *J. Immunol.* **199**, 3360–3368 (2017).
23. E. A. Mroz, J. W. Rocco, MATH, a novel measure of intratumor genetic heterogeneity, is high in poor-outcome classes of head and neck squamous cell carcinoma. *Oral Oncol.* **49**, 211–215 (2013).
24. E. A. Mroz, J. W. Rocco, The challenges of tumor genetic diversity. *Cancer* **123**, 917–927 (2017).
25. C. Schneckenleithner, A. Hoelbl-Kovacic, V. Sexl, Modeling BCR/ABL-driven malignancies in the mouse. *Methods Mol. Biol.* **1267**, 263–282 (2015).
26. H. Lenden Hasse, C. Lescale, J. J. Bianchi, W. Yu, M. Bedora-Faure, L. Deriano, Generation and CRISPR/Cas9 editing of transformed progenitor B cells as a pseudo-physiological system to study DNA repair gene function in V(D)J recombination. *J. Immunol. Methods* **451**, 71–77 (2017).
27. T. Davoli, H. Uno, E. C. Wooten, S. J. Elledge, Tumor aneuploidy correlates with markers of immune evasion and with reduced response to immunotherapy. *Science* **355**, eaaf8339 (2017).
28. H. E. Bhang, D. A. Ruddy, V. Krishnamurthy Radhakrishna, J. X. Caushi, R. Zhao, M. M. Hims, A. P. Singh, I. Kao, D. Rakiec, P. Shaw, M. Balak, A. Raza, E. Ackley, N. Keen, M. R. Schlabach, M. Palmer, R. J. Leary, D. Y. Chiang, W. R. Sellers, F. Michor, V. G. Cooke, J. M. Korn, F. Stegmeier, Studying clonal dynamics in response to cancer therapy using high-complexity barcoding. *Nat. Med.* **21**, 440–448 (2015).
29. L. V. Nguyen, D. Pellacani, S. Lefort, N. Kannan, T. Osako, M. Makarem, C. L. Cox, W. Kennedy, P. Beer, A. Carles, M. Moksa, M. Bilenky, S. Balani, S. Babovic, I. Sun, M. Rosin, S. Aparicio, M. Hirst, C. J. Eaves, Barcoding reveals complex clonal dynamics of de novo transformed human mammary cells. *Nature* **528**, 267–271 (2015).
30. G. Driessens, B. Beck, A. Caauwe, B. D. Simons, C. Blanpain, Defining the mode of tumour growth by clonal analysis. *Nature* **488**, 527–530 (2012).
31. A. Zomer, S. I. Ellenbroek, L. Ritsma, E. Beerling, N. Vrisekoop, J. Van Rheenen, Intravital imaging of cancer stem cell plasticity in mammary tumors. *Stem Cells* **31**, 602–606 (2013).
32. A. Kreso, C. A. O'Brien, P. van Galen, O. I. Gan, F. Notta, A. M. Brown, K. Ng, J. Ma, E. Wienholds, C. Dunant, A. Pollett, S. Gallinger, J. McPherson, C. G. Mullighan, D. Shibata, J. E. Dick, Variable clonal repopulation dynamics influence chemotherapy response in colorectal cancer. *Science* **339**, 543–548 (2013).
33. D. Frumkin, A. Wasserstrom, S. Itzkovitz, T. Stern, A. Harmelin, R. Eilam, G. Rechavi, E. Shapiro, Cell lineage analysis of a mouse tumor. *Cancer Res.* **68**, 5924–5931 (2008).

34. A. Sottoriva, I. Spiteri, S. G. Piccirillo, A. Touloumis, V. P. Collins, J. C. Marioni, C. Curtis, C. Watts, S. Tavaré, Intratumor heterogeneity in human glioblastoma reflects cancer evolutionary dynamics. *Proc. Natl. Acad. Sci. U.S.A.* **110**, 4009–4014 (2013).
35. C. L. Vanderlugt, S. D. Miller, Epitope spreading in immune-mediated diseases: Implications for immunotherapy. *Nat. Rev. Immunol.* **2**, 85–95 (2002).
36. J. Carrasco, A. Van Pel, B. Neyns, B. Lethé, F. Brasseur, N. Renkvist, P. van der Bruggen, N. van Baren, R. Paulus, K. Thielemans, T. Boon, D. Godelaine, Vaccination of a melanoma patient with mature dendritic cells pulsed with MAGE-3 peptides triggers the activity of nonvaccine anti-tumor cells. *J. Immunol.* **180**, 3585–3593 (2008).
37. V. Corbière, J. Chapiro, V. Stroobant, W. Ma, C. Lurquin, B. Lethé, N. van Baren, B. J. Van den Eynde, T. Boon, P. G. Coulie, Antigen spreading contributes to MAGE vaccination-induced regression of melanoma metastases. *Cancer Res.* **71**, 1253–1262 (2011).
38. M. DuPage, C. Mazumdar, L. M. Schmidt, A. F. Cheung, T. Jacks, Expression of tumour-specific antigens underlies cancer immunoediting. *Nature* **482**, 405–409 (2012).
39. H. Matsushita, M. D. Vesely, D. C. Koboldt, C. G. Rickert, R. Uppaluri, V. J. Magrini, C. D. Arthur, J. M. White, Y. S. Chen, L. K. Shea, J. Hundal, M. C. Wendl, R. Demeter, T. Wylie, J. P. Allison, M. J. Smyth, L. J. Old, E. R. Mardis, R. D. Schreiber, Cancer exome analysis reveals a T-cell-dependent mechanism of cancer immunoediting. *Nature* **482**, 400–404 (2012).
40. L. von Boehmer, M. Mattle, P. Bode, A. Landshammer, C. Schäfer, N. Nuber, G. Ritter, L. Old, H. Moch, N. Schäfer, E. Jager, A. Knuth, M. van den Broek, NY-ESO-1–specific immunological pressure and escape in a patient with metastatic melanoma. *Cancer Immun.* **13**, 12 (2013).
41. T. Nicholaou, W. Chen, I. D. Davis, H. M. Jackson, N. Dimopoulos, C. Barrow, J. Browning, D. Macgregor, D. Williams, W. Hopkins, E. Maraskovsky, R. Venhaus, L. Pan, E. W. Hoffman, L. J. Old, J. Cebon, Immunoediting and persistence of antigen-specific immunity in patients who have previously been vaccinated with NY-ESO-1 protein formulated in ISCOMATRIX. *Cancer Immunol. Immunother.* **60**, 1625–1637 (2011).
42. C. Roche-Lestienne, J. L. Laï, S. Darré, T. Facon, C. Preudhomme, A mutation conferring resistance to imatinib at the time of diagnosis of chronic myelogenous leukemia. *N. Engl. J. Med.* **348**, 2265–2266 (2003).
43. D. A. Landau, S. L. Carter, P. Stojanov, A. McKenna, K. Stevenson, M. S. Lawrence, C. Sougnez, C. Stewart, A. Sivachenko, L. Wang, Y. Wan, W. Zhang, S. A. Shukla, A. Vartanov, S. M. Fernandes, G. Saksena, K. Cibulskis, B. Tesar, S. Gabriel, N. Hacohen, M. Meyerson, E. S. Lander, D. Neuberg, J. R. Brown, G. Getz, C. J. Wu, Evolution and impact of subclonal mutations in chronic lymphocytic leukemia. *Cell* **152**, 714–726 (2013).
44. C. G. Mullighan, L. A. Phillips, X. Su, J. Ma, C. B. Miller, S. A. Shurtleff, J. R. Downing, Genomic analysis of the clonal origins of relapsed acute lymphoblastic leukemia. *Science* **322**, 1377–1380 (2008).
45. J. M. Zaretsky, A. Garcia-Diaz, D. S. Shin, H. Escuin-Ordinas, W. Hugo, S. Hu-Lieskovan, D. Y. Torrejon, G. Abril-Rodriguez, S. Sandoval, L. Barthly, J. Saco, B. Homet Moreno, R. Mezzadra, B. Chmielowski, K. Ruchalski, I. P. Shintaku, P. J. Sanchez, C. Puig-Saus, G. Cherry, E. Seja, X. Kong, J. Pang, B. Berent-Maoz, B. Comin-Anduix, T. G. Graeber, P. C. Tumeh, T. N. Schumacher, R. S. Lo, A. Ribas, Mutations associated with acquired resistance to PD-1 blockade in melanoma. *N. Engl. J. Med.* **375**, 819–829 (2016).
46. N. Riaz, J. J. Havel, V. Makarov, A. Desrichard, W. J. Urba, J. S. Sims, F. S. Hodi, S. Martin-Algarra, R. Mandal, W. H. Sharfman, S. Bhatia, W. J. Hwu, T. F. Gajewski, C. L. Slingluff Jr., D. Chowell, S. M. Kendall, H. Chang, R. Shah, F. Kuo, L. G. T. Morris, J. W. Sidhom, J. P. Schneck, C. E. Horak, N. Weinhold, T. A. Chan, Tumor and microenvironment evolution during immunotherapy with nivolumab. *Cell* **171**, 934–949. e16 (2017).
47. L. G. Morris, N. Riaz, A. Desrichard, Y. Senbabaoğlu, A. A. Hakimi, V. Makarov, J. S. Reis-Filho, T. A. Chan, Pan-cancer analysis of intratumor heterogeneity as a prognostic determinant of survival. *Oncotarget* **7**, 10051–10063 (2016).
48. A. Valujskikh, O. Lantz, S. Celli, P. Matzinger, P. S. Heeger, Cross-primed $CD8^+$ T cells mediate graft rejection via a distinct effector pathway. *Nat. Immunol.* **3**, 844–851 (2002).
49. C. Lescale, V. Abramowski, M. Bedora-Faure, V. Murigneux, G. Vera, D. B. Roth, P. Revy, J. P. de Villartay, L. Deriano, RAG2 and XLF/Cernunnos interplay reveals a novel role for the RAG complex in DNA repair. *Nat. Commun.* **7**, 10529 (2016).
50. N. Rosenberg, D. Baltimore, C. D. Scher, In vitro transformation of lymphoid cells by Abelson murine leukemia virus. *Proc. Natl. Acad. Sci. U.S.A.* **72**, 1932–1936 (1975).
51. I. B. Mazo, J. C. Gutierrez-Ramos, P. S. Frenette, R. O. Hynes, D. D. Wagner, U. H. von Andrian, Hematopoietic progenitor cell rolling in bone marrow microvessels: Parallel contributions by endothelial selectins and vascular cell adhesion molecule 1. *J. Exp. Med.* **188**, 465–474 (1998).

Acknowledgments: We thank the members of the Bousso laboratory for critical review of the manuscript and D. Michonneau, M. Almena, J. Postat, C. Grandjean, B. Breart, F. Lemaître, S. Celli, and M. Cazaux for help with some experiments. We acknowledge the animal facility and the cytometry platform of Institut Pasteur for help with cell sorting and the specific contribution of S. Novault and S. Schmutz. **Funding:** This work was supported by Institut Pasteur, Inserm, a grant from the Pasteur-Weizmann Council, a grant from the Fondation de France, the Institut National du Cancer (no. PLBIO16-181 to L.D.), and the European Research Council (starting grant LymphocyteContacts and advanced grant ENLIGHTEN to P.B. and starting grant LymphoOncoGenomics to L.D.). **Author contributions:** I.M., L.D., and P.B. conceived and designed the study. I.M., M.B.-F., Z.G., and R.T. performed the experiments. I.M., M.B.-F., L.D., and P.B. analyzed the data. G.S. and L.P. provided conceptual insights. I.M. and P.B. wrote the manuscript. **Competing interests:** The authors declare that they have no competing interests. **Data and materials availability:** Exome sequencing raw data were deposited in the Sequence Read Archive (SRA) database (SRA accession no. PRJNA494854).

Submitted 29 January 2018
Resubmitted 3 August 2018
Accepted 18 October 2018
Published 23 November 2018
10.1126/sciimmunol.aat1435

Citation: I. Milo, M. Bedora-Faure, Z. Garcia, R. Thibaut, L. Périé, G. Shakhar, L. Deriano, P. Bousso, The immune system profoundly restricts intratumor genetic heterogeneity. *Sci. Immunol.* **3**, eaat1435 (2018).

Science Immunology

The immune system profoundly restricts intratumor genetic heterogeneity

Idan Milo, Marie Bedora-Faure, Zacarias Garcia, Ronan Thibaut, Leïla Périé, Guy Shakhar, Ludovic Deriano and Philippe Bousso

Sci. Immunol. **3**, eaat1435.
DOI: 10.1126/sciimmunol.aat1435

Immunoediting of polychromatic tumors

As tumors grow, they evolve genetically. The resulting genetic heterogeneity contributes to the emergence of variants that may ultimately display increased resistance to immune effector mechanisms and enhanced metastatic potential. Milo *et al*. used multicolor barcoding of a mouse lymphoma line to determine whether increased immune selection pressure by the host accelerates the emergence of dominant clones. When barcoded male lymphoma cells were given to male and female recipients, clonal dominance emerged more rapidly in female recipients because more neoantigens were available to elicit a host T cell response. Checkpoint blockade with anti–PD-1 promoted a similar contraction of intratumor diversity. These findings provide fresh insights into the immunoediting mechanisms by which active antitumor immunity directs the in vivo selection of less immunogenic tumor variants.

Science Immunology (ISSN 2470-9468) is published by the American Association for the Advancement of Science, 1200 New York Avenue NW, Washington, DC 20005. The title *Science Immunology* is a registered trademark of AAAS.